JOURNAL OF MATERIALS SCIENCE 32 (1997) 4331–4346

Indentation brittleness of ceramics: a fresh approach

J. B. QUINN
Department of Engineering Materials, University of Maryland, College Park, MD 20742, USA

G. D. QUINN
Ceramics Division, National Institute of Standards and Technology, Gaithersburg, MD 20899, USA

The hardness and brittleness of ceramic materials are interrelated. Hard materials are more apt to fracture in the vicinity of an indentation during a hardness test, while softer materials tend to plastically deform to the indenter shape without fracturing. Measured hardness, in turn, is affected by both specimen deformation and fracture processes. This interrelationship is examined by means of extensive Vickers hardness testing. A new index of brittleness is proposed.

1. Introduction

Ceramics are generally associated with distinctive properties, some uniquely beneficial and some restrictive, which determine the materials' utilities. Among these are hardness, brittleness and fracture toughness. The measured hardness of a brittle material as determined by conventional tests (Vickers, Knoop, Berkovich, Rockwell, etc.) is a measure of a material's resistance to deformation, densification, displacement and fracture.

Conventional hardness measurements, which depend on the size of an indentation resulting from an applied load, are load dependent. This is especially noticeable at lower indentation loads where most measurements are made in order to avoid experimental problems associated with fracture. Local fracture around and under an indentation can affect the depth of penetration or size of the indentation and thus can be considered an intrinsic part of the indentation process. Fracture also can create practical difficulties in making hardness measurements because cracking at indentation corners or fragmentation can hamper or preclude plausible hardness measurements. The degree of fracture at indentations in ceramics is load dependent. Low loads are associated with deformation, while fracture is conspicuously more prominent at high loads.

This paper examines the relationships between hardness, load and fracture from an unconventional viewpoint. The well known and pronounced hardness–load dependency of ceramic materials is first reviewed, and then the relationship between hardness and fracture is explored. A new index of brittleness, based on fracture energy and deformation energy ratios, is proposed.

1.1. The hardness–load dependency

Hardness is conventionally determined by applying a load to a material via a geometrically defined indenter, usually a steel or diamond ball or a diamond pyramid. The ratio of this load to the contact (or projected) area of the resultant impression is defined as the hardness, H

$$H = \alpha \frac{P}{d^2} \tag{1}$$

where P is the applied load; d is the size of the measured impression; and the indenter constant, α, depends on the indenter geometry. The hardness of a material is often characterized by a single numerical value, an example being the hardness often provided in company product sheets. For ceramics, this is generally the Vickers or Knoop hardness. When a very low test load is applied to a ceramic, the measured hardness is usually very high. With an increase in load, however, the measured hardness decreases [1–6] as illustrated in Fig. 1a. At higher indentation loads, hardness–load curves for ceramic specimens flatten out and hardness becomes constant. Despite the well known dependency of hardness on load, however, published hardness values seldom include the load at which the hardness was assessed. A full hardness characterization by a hardness–load curve is uncommon in ceramics. Furthermore, there are no relationships or tables for converting different hardness test values, such as Knoop to Vickers hardness, or vice-versa. Hardness comparisons of ceramic materials must be approached with knowledgeable caution.

The specification of a single, universal test load for Vickers measurements (e.g. as in a standard) has a number of drawbacks including that cracking may or may not manifest itself at the designated load in different ceramic materials. It may be misleading to compare the hardness of one material that has cracked to the hardness of another that has not cracked. The cracking may influence the hardness in the former

0022–2461

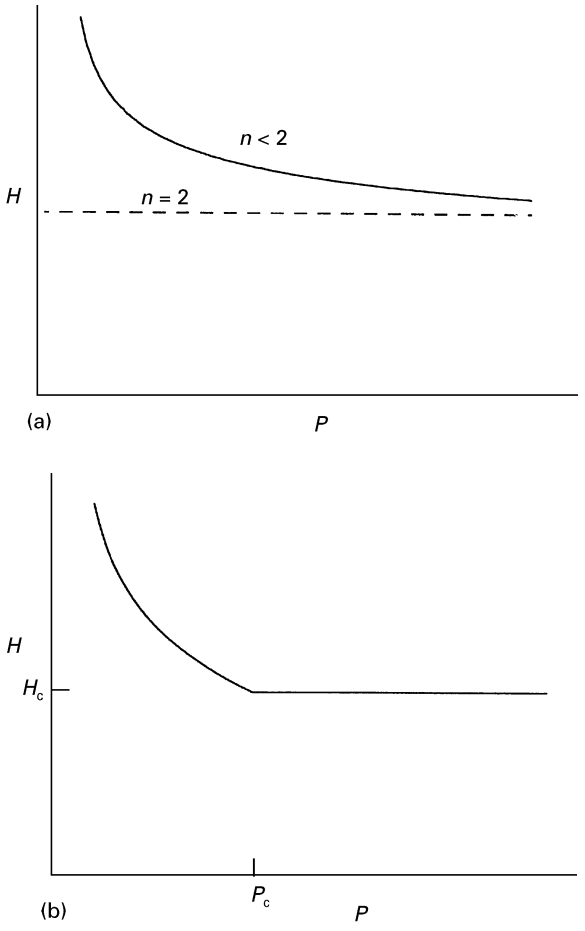

Figure 1 Hardness versus load: (a) shows hardness either constant ($n = 2$) or decreasing with load ($n < 2$), and (b) shows hardness with an abrupt transition to a constant value at (P_c, H_c).

material, or in the extreme, may make the indent unreadable. (For example, 9.8 N Vickers indents in a silicon carbide will be very different than those in a zirconia.) The Knoop test, with a much shallower indentation, is less susceptible to cracking problems and thus has a broader range at which readable hardness impressions are possible. Generalizations concerning comparisons of Knoop hardness to Vickers hardness are difficult due to the different propensities for cracking and different sensitivities to load and indenter geometry.

Plots of hardness versus load data are sometimes fitted to the Meyer law, which was originally used to determine the work-hardening capacity of metals in Brinell hardness tests [5, 7]. Although there exists no theoretical basis for applying the Meyer law to Knoop and Vickers generated hardness–load curves [8], a good empirical fit can sometimes be attained by doing so. The Meyer law is

$$P = Cd^n \tag{2}$$

where P is the load, C is a constant, d is the measured impression size, and n is the Meyer or logarithmic index denoting the degree of curvature for the hardness–load relationship. By combining Equations 1 and 2, it can be seen that if $n = 2$, hardness does not change with load, and a hardness–load graph is flat. If $n < 2$, then hardness decreases with increasing load, and as Sargent [6] has pointed out, the constant C is a material parameter with the strange units of $N\,m^{-n-1}$. Fig. 1a illustrates the hardness–load curves for $n = 2$ and $n < 2$.

The hardness–load curve itself, or sometimes the Meyer index that characterizes the curve, is often referred to as the indentation size effect, or ISE. The ISE has also come to denote the general tendency for hardness to vary with load. This effect is especially apparent in hard, brittle ceramics at low indentation loads, where n is significantly less than 2.

Close scrutiny of Vickers hardness–load curves for ceramics, such as those shown in [3, 4, 9–17], suggests a discrete transition point may exist where hardness changes from being load dependent to load independent as illustrated in Fig. 1b. We contend that this transition point, which is nearly always overlooked, is intimately associated with the onset of extensive fracture in the vicinity of the indentation. The verification and interpretation of this transition is the primary focus of this paper.

Equation 2 does not predict a transition point to constant hardness, and the common practice of forcing the Meyer law to data masks such a point. Many ceramics are not well modelled by the Meyer analysis. This is especially the case for Vickers hardness, which fits the Meyer model less well than Knoop hardness [18]. Experimental error, plotting methodology and the simple expectation of a continuous curve further contribute to the lack of interest in discerning the existence of a discrete transition point.

The inadequacy of the Meyer analysis has prompted alternative attempts to achieve improved curve fits to hardness–load or hardness–indentation size data. Bückle [19] and Mitsche [20] suggested a power series expansion

$$P = a_0 + a_1 d + a_2 d^2 + \ldots a_n d^n \tag{3}$$

where P is the load, d is the indentation diagonal size, and a is a constant. A good fit to experimental data is often obtained utilizing only two of the power series terms. This results in a formula that Fröhlich *et al.* [21] and Li and Bradt [2] ascribe to Bernhardt [22]

$$P = a_1 d + a_2 d^2 \tag{4}$$

(Bernhardt did not write an equation in this form explicitly, but it is clear from his text that this was the intent. Note also that the depth of the indenter penetration, l, is proportional to d, and thus Equation 4 can also be expressed as $P = b_1 l + b_2 l^2$.)

The a_0 term corresponds to a load threshold for an indenter to make a permanent indentation, and has such a low magnitude that it can be ignored in most instances. This simple, yet versatile relationship between load and indentation size can be re-expressed several ways. It can be rewritten in units of hardness by dividing by d^2

$$\frac{P}{d^2} = \frac{a_1}{d} + a_2 \tag{5}$$

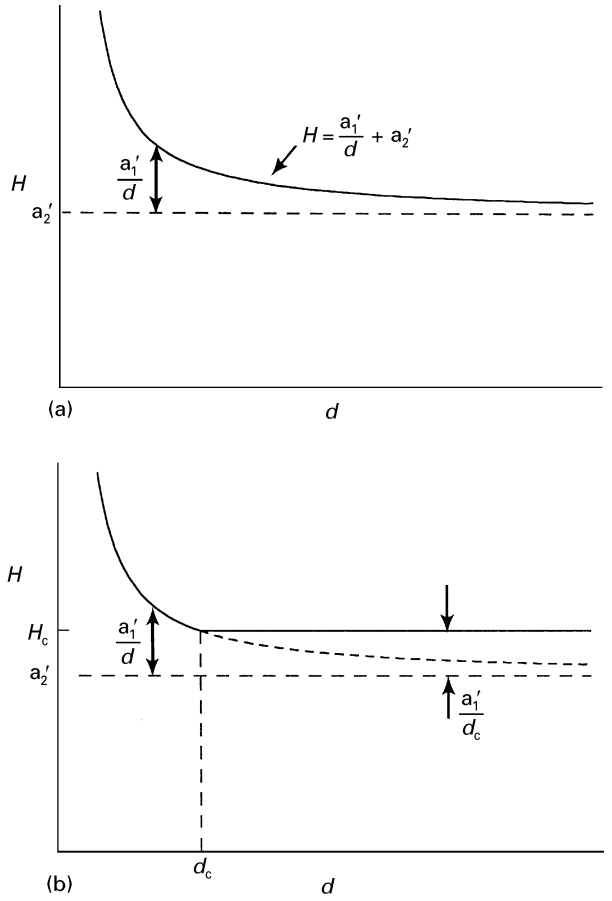

Figure 2 Hardness versus diagonal size: (a) shows behaviour modelled by Equation 6. The indentation size effect comes from the a_1'/d term. (b) Shows hardness with a transition to constant hardness at a critical indentation size.

or, using the definition of hardness, Equation 1

$$H = \frac{a_1'}{d} + a_2' \tag{6}$$

where the prime indicates that the indenter constant (1.8544 for a Vickers indenter) is incorporated into the constants a_1 and a_2. Equation 6 is illustrated in Fig. 2a.

Comparing Equations 2 and 4, it can be seen that the second term on the right-hand side of Equation 4, $a_2 d^2$, is identical to the right-hand side of Equation 2, but only if $n = 2$, which corresponds to the hardness being load independent. Thus, in Equations 4 –6, the terms with a_2 or a_2' do not contribute to an ISE. It is the first term on the right-hand side of these equations, or the term with a_1 or a_1', that determines the amount of curvature or magnitude of the ISE as shown in Fig. 2a.

The relationship between indentation load and indentation diagonal size, Equation 4, alternatively may be re-expressed as an energy balance by multiplying both sides by d

$$Pd = a_1 d^2 + a_2 d^3 \tag{7}$$

As will be discussed later, the term Pd may be related to the external work done by the indenter. Fröhlich *et al.* [21] and Bernhardt [22] relate the $a_1 d^2$ term to the energy consumed in creating new surfaces (indentation facets and microfracture). Hirao and Tomozawa [23] have also attempted to correlate surface energy processes to this term, while Li and coworkers [24, 25] have related this term to frictional and elastic contributions in a proportional specimen resistance (PSR) model. Swain and Wittling [26] attributed the ISE to the $a_1 d^2$ term and argued that median cracks under Knoop indentations were the source of the ISE.

The $a_2 d^3$ term, on the other hand, is thought to be the "work of permanent deformation" [21] or the "volume energy of deformation" [25]. The analogous a_2' constant is related to the "crack free hardness, (L2VH)" by Fröhlich *et al.* [21] and Frischat [27], the "load-independent hardness" by Li and Bradt [24] or represents the "true hardness" by Hirao and Tomozawa [23].

Equations 4–6 do not predict a specific, discrete transition point to constant hardness. In either the energy or PSR models, the apparent fit of the data to these equations fosters the tendency to overlook the existence of an abrupt transition point.

Other mechanisms proposed to explain the ISE are elastic recovery [28, 29], surface damage due to polishing [30], dislocation activity [31] and strain rate effects [1]. As noted by Li *et al.* [25], the different mechanisms seem to work for specific situations. It is likely that all these mechanisms play a role in ISE, for they are not mutually exclusive and material and test characteristics may affect the order and degree of mechanism dominance.

1.2. Hardness and fracture

A more general approach is to regard the ISE as a total indentation response with both deformation and fracture processes active. Deformation is the controlling characteristic at low loads, and fracture gradually becomes relevant at higher loads. There has been considerable work in recent years on cracks associated with hardness impressions [30, 32–37]. Most of these studies have focused on the micromechanics of fracture and are concerned with the formation and propagation of specific, moderate-sized cracks beneath indentations. Vickers indentations have been widely used for these studies, although there has been similar research employing Knoop indentations [11, 37, 38]. In a series of papers, Lawn and coworkers [32, 39– 42] showed how indentations change from deformation dominated behaviour to fracture dominated behaviour above threshold load levels. A number of crack types (median, radial, lateral, cone, etc.) are possible depending upon the indenter sharpness and geometry, and each has associated with it a different functional relationship between load, hardness, fracture toughness and crack size [41, 43, 44]. Extrapolation of load and crack size data (from high to low load) is used to determine fracture initiation and propagation parameters in these idealized crack systems. Below a load threshold, the cracks will not form. A different load threshold, or fracture transition point, is thus defined for each type of crack.

We suggest that a transition to fracture orientated behaviour may not necessarily be heralded by the initiation of an idealized, specific type of crack, or even by clearly delineated cracks at all. A general damage zone with non-specific microcracking, for example, may develop in some materials; other materials may be prone to extensive, but hidden, subsurface cracking. Even the appearance of classical surface cracking patterns may not always signify the true extent of the fracture response to the applied load.

While difficult to identify via surface crack inspection, we propose that the onset of brittle, fracture dominated behaviour may be determined by an alternate method, involving a transition point in hardness–load curves. The previously cited fracture mechanics studies have thus far emphasized the effect of load and hardness on fracture processes and fracture toughness. They have not considered in detail the reverse effect of fracture on *hardness*.

1.3. Hardness: an energy balance model

A general energy balance for a Vickers indentation process may be formulated in which the external work applied by the indenter is consumed in deformation and fracture processes in a material. The work of indentation is converted into a strain energy component, proportional to the Vickers pyramid volume, and a surface energy component, proportional to the Vickers pyramid contact area, and created fracture surface area.

We begin with Equation 7, which is an energy balance for the indentation process consistent with a dimensional analysis. Pd is proportional to the work of indentation which is $\int Pdl$, where P is the applied load and l is the penetration depth. Graphs of load versus penetration depth during indentations of dense ceramics [26, 27, 45–47] indicate the curves are similar in shape, and the work of indentation is proportional to Pl and thus also to Pd. (The proportionality constants are included in a_1 and a_2. The elastic component of the indentation process may be either included or excluded in the energy balance depending upon whether the indentation depth or diagonal sizes are measured with the indenter in contact under full load, or after indenter removal. For the remainder of this paper, the depths or diagonal sizes are the permanent values and do not include the elastic component.) Note that the total work of indentation is proportional to Hd^3, and the work per unit volume is proportional to H. [$H = P/(\text{indent area}) = Pl/(\text{indent area} \times l)$ = work done by indenter/(3 × volume of indentation) since the volume of the pyramidal impression is $\frac{1}{3}$ base area × height.] The hardness, therefore, is a measure of the specific work of indentation.

The second term in Equation 7, the a_1d^2 term, represents energy expended in the material in the process of creating new surface area. Among the contributions to the surface energy is the new area formed by the four facets of the pyramidal indenter. This component, which is proportional to the thermodynamic free surface energy, γ_s, is quite small. This is shown by considering the indentation contact surface area of a Vickers indenter, $(1/1.8544)d^2$. The surface it replaces is the flat specimen area that existed before the indent, $(1/2)d^2$, and thus the change in indentation surface area is only $(1/1.8544)d^2 - (1/2)d^2 = 0.0393d^2$. Frictional effects also depend upon the indenter contact area and mounting evidence suggests this contribution to be higher than previously recognized [24, 25]. If fracture occurs, fracture surface area creation will also consume some of the work of indentation and this energy contribution will be proportional to the fracture surface energy, γ_f. Microcracks and damage zones are frequently discernible throughout the hardness testing range of a ceramic specimen, even at very low loads [9, 27, 48–50]. Although marked fracture may not be apparent until higher loads are applied, even relatively small microcracks at the corners of a Vickers impression can account for a significant increase in new surface area compared with the new surface area created by the impression itself. Microfissuring directly underneath and alongside the indenter also appears to be extensive [51]. The energy model assumes that the new crack area is proportional to the surface area of the Vickers impression. (Some of the microfracturing will be in the plastically deformed volume directly below the indentation, and in this case, a portion of the fracture energy would be included in the volume term, a_2d^3.)

The third term in Equation 7 represents the volume energy component, a_2d^3, which includes the material deformation resulting from the indentation, and may be expressed in terms of a specific strain energy times the deformation volume. a_2 presumably is proportional to the yield stress, σ_y. The energy consumed in plastically deforming the material is related to the stresses and strains in the deformation zone, but these are triaxial and complicated to analyse in detail.

1.3.1. Energy ratio at low load, $d < d_c$

Starting at low applied loads, the indentation work is absorbed by volume deformation processes (the a_2d^3 term) and by modest surface energy absorption processes (the a_1d^2 term). The existence of the latter prevents the formation of indentations as large as they otherwise would be if all energy were consumed in the volume deformation.

As load is increased, the indentations become larger and more energy is absorbed via volume deformation and crack propagation, i.e. an increasing volume of material is deformed and an increasing crack surface area is generated. The former increases more rapidly than the latter, however, due to the different dependencies (cubed versus squared power) upon indentation size. The hardness continues to decrease with load until a transition to constant hardness is reached. At this point, the ratio of surface energy consumption to total indentation work reaches a critical ratio, β_c

$$\beta_c = \frac{a_1 d_c^2}{P_c d_c} \tag{8}$$

or:

$$\beta_c = \frac{(a_1/d_c)}{(P_c/d_c^2)} = \frac{(a_1'/d_c)}{H_c} \tag{9}$$

where H_c denotes the hardness of the material at d_c, and as before, the indenter diamond constant is incorporated in a'_1. H_c, P_c and d_c correspond to the hardness, load and diagonal sizes at the transition point to constant hardness as shown in Figs 1b and 2b.

Equation 9 illustrates that β_c is not only a critical energy ratio, but is a critical hardness ratio as well. It represents the ratio of the hardness component that is involved with surface energy consumption processes to the total hardness. If we assume that a_1 is proportional to the thermodynamic surface free energy, γ_s, and the effective fracture surface energy, γ_f, and that these are proportional, then

$$\beta_c = \frac{A(\gamma_f/d_c)}{H_c} \quad (10)$$

where A is a constant. For plane strain

$$K_{Ic} = \left[\frac{2E\gamma_f}{(1-\nu^2)}\right]^{1/2} \quad (11)$$

where E is Young's modulus, ν is Poisson's ratio, and K_{Ic} is the fracture toughness. Substituting in Equation 10

$$\beta_c = A'\frac{(K_{Ic}^2/d_c)}{H_c E} \quad (12)$$

where A′ is a new constant incorporating A, the factor of two and $(1-\nu^2)$. Rearranging

$$d_c = \frac{A'}{\beta_c}\left(\frac{K_{Ic}^2}{H_c E}\right) \quad (13)$$

and inverting

$$\frac{1}{d_c} = \frac{\beta_c}{A'}\left(\frac{H_c E}{K_{Ic}^2}\right) \quad (14)$$

The combination of material parameters in the brackets is a new parameter that we define as brittleness, B

$$B \equiv \left(\frac{H_c E}{K_{Ic}^2}\right) \quad (15)$$

and which will be discussed in detail in the following sections. We hypothesize that the hardness transition point corresponds to the onset of extensive cracking around and beneath the indentation. The onset of such cracking occurs at a critical energy balance in the system. The indentation system may be described as saturated, i.e. it has reached its maximum capacity to convert indentation work into surface energy by microcracking or microfissuring in the immediate vicinity of the indentation. The extensive or new cracking that commences at the transition point may or may not necessarily correspond to one of the classical crack patterns (radial, median or lateral) in the fracture mechanics models described previously. Gross cracking and crushing are typical at indentation loads where hardness becomes load independent [13, 44, 52].

1.3.2. Energy ratio at high loads, $d > d_c$

At indentation loads and indentation sizes above the transition point, a new surface energy absorption term comes into play. In order to maintain a constant hardness at $d > d_c$, the new mechanism of energy absorption must operate to offset the decrease in magnitude of the a'_1/d term as the indentation load and diagonal size increase.

Fig. 2a shows behaviour according to Equation 6, indicating that at large d values a'_1/d decreases asymptotically towards a'_2, effectively vanishing. However, as hardness is load- independent and therefore constant at $d > d_c$, a new constant magnitude surface energy term, a'_1/d_c has to become operative at $H = H_c$, which is additive to the load independent hardness component, a'_2, as illustrated in Fig. 2b. (The a'_1/d_c term either replaces the a_1/d term of Equation 6, or gradually phases in at $d > d_c$ to offset the continued diminishment of a_1/d as discussed in Appendix I.) Thus, Equation 6 is modified to

$$H = a'_2 + \frac{a'_1}{d_c} \quad (16)$$

Multiplying both sides by d^3 leads to

$$Pd = a_2 d^3 + \frac{a_1}{d_c} d^3 = a_2 d^3 + a_4 d^3 \quad (17)$$

where $a_4 = a_1/d_c$. The energy (and hardness) ratio β for $d > d_c$ is thus

$$\beta_{d>d_c} = \frac{(a_1/d_c)d^3}{Pd} = \frac{(a_1/d_c)}{(P/d^2)} = \frac{(a'_1/d_c)}{H_c} \quad (18)$$

where we note that P/d^2 is constant ($H = H_c$) for $d \geqslant d_c$. This β ratio is the same as that at the critical transition point, $d = d_c$. The difference, however, is that as the indentation load and diagonal size increase, the term in the energy balance that pertains to fracture, $a_4 d^3$, now increases as the cube of the indentation size and not as the square. (For $d < d_c$, the total fracture surface area created was assumed to be proportional to the indentation diagonal size squared, or indenter contact area. For $d > d_c$, the fracture surface area expands faster than the indentation contact area.) This term includes not only the fracture surface energy, γ_f, but geometrical factors (the number of cracks, their size and their shape), and the actual surface area of the cracks. In other words, the extent of post-threshold cracking dramatically increases.

The existence of a constant hardness transition point can be investigated experimentally. Although numerous experiments have already been reported in the literature in order to evaluate the ISE constants of the Meyer law, Equation 2, or the alternative Equations 4 or 6, none of these studies have been specifically orientated towards determining an abrupt transition to constant hardness.

2. Experimental procedure

Seven well characterized dense polycrystalline ceramics exhibiting a measurable ISE were chosen to

TABLE I Materials tested[a,b]

Material[c]	ρ ($Mg\,m^{-3}$)	E (GPa)	K_{Ic}[d] ($MPa\,m^{-1/2}$)	Vickers hardness HV_c (GPa)	d_c (μm)	P_c (N)	B (μm^{-1})
Al_2O_3 AD999, Coors sintered [55, 56]	3.96	386	4.0 (SCF, other)	18.2	45.9	20.7	439
Pyroceram 9603, Corning [53–56]	2.64	134	2.4 (CM–DCB)	6.8	125.0	57.3	157
α-SiC, carborundum sintered [55–57]	3.11	410	3.0 (SCF)	22.6	20.2	5.0	1023
Si_3N_4 NC132, Norton hot pressed [55–57]	3.23	320	4.6 (SCF, other)	15.4	78.9	51.7	233
Si_3N_4 NBD200, Norton hot isopressed [55, 56]	3.16	320	5.4 (SCF)	14.9	120.0	116.0	163
Si_3N_4 NT154, Norton hot isopressed [55, 56]	3.23	315	5.8 (SCF)	14.9	114.0	105.0	140
α-SiC, carborundum sintered [12, 58]	3.16	430	3.0 (CN, SCF, other)	27.0	14.5	3.1	1290
ALON, Army Research Laboratory aluminum oxynitride spinel [16]	3.61	320	2.75 (SB–CN, NAT, other)	14.6	31.1	7.6	618

[a] Certain commercial equipment, instruments or materials are identified in this paper in order to specify the experimental procedure adequately. Such identification does not imply recommendation or endorsement by the National Institute of Standards and Technology, nor does it imply that the materials are necessarily the best for the purpose.
[b] The uncertainties for the parameters vary somewhat with material. Expressed as the coefficient of variation in per cent, the uncertainties are approximately: E, ± 1%; K_{Ic}, ± 5%; HV_c, ± 1.5%; d_c, ± 5%; P_c, ± 10%; and B, ± 10%.
[c] The source references for the ρ, E and K_{Ic} data are shown in parentheses.
[d] The notations in parentheses are the test method: (CN) chevron notch, (SB–CN) short bar–chevron notch, (SCF) surface crack in flexure (controlled surface flaw), (CM–DCB) constant moment double cantilever beam, (NAT) fractography, natural flaws. (Other): denotes original reference has corroborative data by other methods.

determine whether hardness does reach a plateau and whether the transition point correlated to a critical energy ratio and the material constants in Equations 13 and 14. The materials are listed in Table I. One of the reasons these materials were chosen was that the fracture toughnesses were very well characterized. Hardness–load curves for the first six entries were expressly performed for this study. Data for density, ρ, Young's modulus, E, and fracture toughness, K_{Ic}, are taken from the listed sources. The second entry for sintered silicon carbide uses data entirely from Li *et al.* [12] and Ghosh *et al.* [58]. The data are listed separately for reasons that will be discussed below. All data, including hardness, for the aluminum oxynitride spinel are from [16].

These materials have a range of material properties and, with the possible exception of the NT 154, are known to have no (or negligible) R-curve behaviour. They also were sufficiently fine grained to limit grain-size effects in the ISE, and avoid excessive scatter in the data at small indentation impressions. The materials are also relatively impervious to ambient environmental effects. (Alumina has been shown to exhibit a noticeable environmental effect only at loads below 100 g in Vickers tests [59]).

Specimens were polished to an optical finish (0.25 μm diamond). The polished specimens were tested on a Tukon Model 300 hardness testing machine with a Vickers indenter for loads up to 98 N. The Tukon 300 was equipped with a digital microhardness display unit with an electronic filar eyepiece enabling Vickers diagonals to be measured with a precision of better than 0.5 μm. Loads exceeding 98 N were applied with a Zwick 3 212 001/00 hardness tester, with the resulting indentations measured on the Tukon 300 optical system for consistency. Duplicate indentations were made using both hardness machines at loads of 49 and 98 N in order to ensure there was no systematic bias between the machines. A minimum of five hardness readings (but often many more) were taken at each load, with the unreadable indentations at high loads redone until acceptable impressions were obtained. Considerable care was taken in all aspects of measuring the Vickers diagonals. This point cannot be underestimated, because if proper care is not taken, important ISE or transition point behaviour may be obscured or lost by data scatter [60–62]. For example, Clinton *et al.* [63] illustrated how different observers obtained different hardness–load curves for the identical alumina in a single laboratory with the same instrument. One observer's results showed a clear plateau, the other observer's results illustrated a different trend that was attributed to small errors of measurement. Beyond the hardness transition point, and on the constant hardness plateau, cracking around the indentation can severely interfere with or obviate measurements of the indentation size. At high loads in some of the materials tested it was necessary to make many indentations until a few measurable indentations were obtained. It was also prudent to measure the indentations as soon as possible after indentation before any spalling or time dependent cracking occurred. While simple in concept, hardness testing is fraught with experimental pitfalls that often are not appreciated. Hardness measurements are very sensitive to machine vibrations, optical microscope limitations (resolution limits, illumination conditions, crosshair technique, etc.) and operator subjectivity

and skill. A recent round robin project [60] on Vickers hardness of two aluminas at 9.8 N demonstrated that laboratory to laboratory variations in mean hardness of $\pm$ 10–15% were typical (and in some cases as much as 20%). Testing machine calibration should be checked frequently and use of certified reference materials is highly recommended [61, 62].

The hardness–load data for one of the materials, NC132 Si_3N_4, were independently determined by both authors in this study in order to confirm the constant hardness transition point and the repeatability of the experiments.

Hardness values were calculated from the standard Vickers formula

$$HV = 1.8544\ P/d^2 \quad (19)$$

where HV is the Vickers hardness, P the applied load and d the measured diagonal. The conventional definition of Vickers hardness, HV, is applied load divided by contact area. Every official *standard* test method and every Vickers *standard* hardness (certified) reference material in the world use this definition, as do most textbooks on hardness testing. The constant hardness transition points were determined by inspection of the hardness–load graphs (plotted on linear, *not* logarithmic axes). Separate linear regression analyses of the data segments for $d < d_c$ and $d > d_c$ were made to obtain P_c, the critical transition point load. The transition diagonal, d_c, was then calculated from Equation 1 using $H = H_c$.

3. Results

The hardness–load data for the six tested materials were first plotted on linear hardness–load axes, comprising Figs 3–8. The error bars are plus and minus one standard deviation in each case. All six materials exhibited distinct hardness transitions and plateaus. The ISE at low loads appears nearly linear in all of these plots prior to a constant hardness transition. Table I lists the constant hardness and the Vickers diagonals at which the constant hardness transitions occur for the five materials.

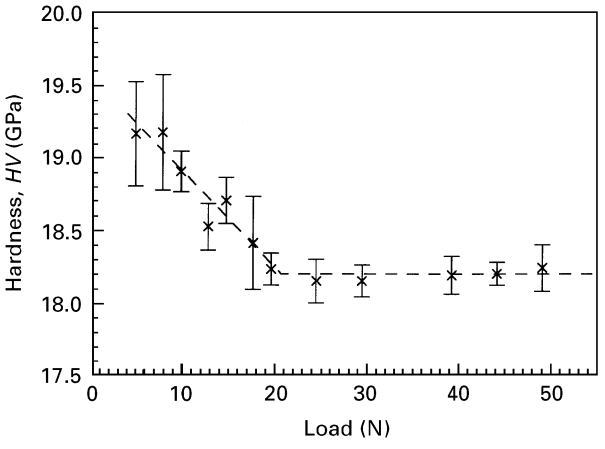

Figure 3 Hardness as a function of load for AD999 alumina.

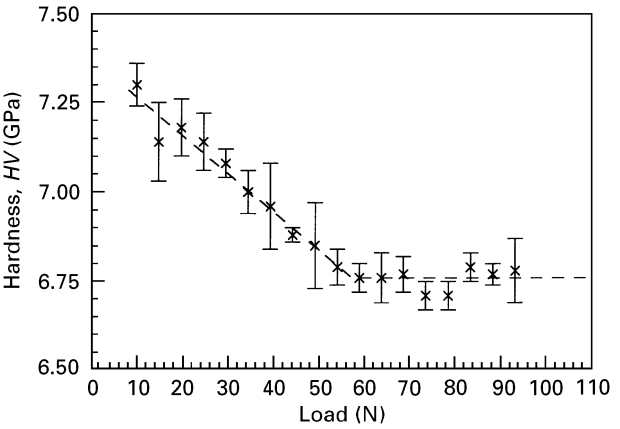

Figure 4 Hardness as a function of load for Pyroceram 9603.

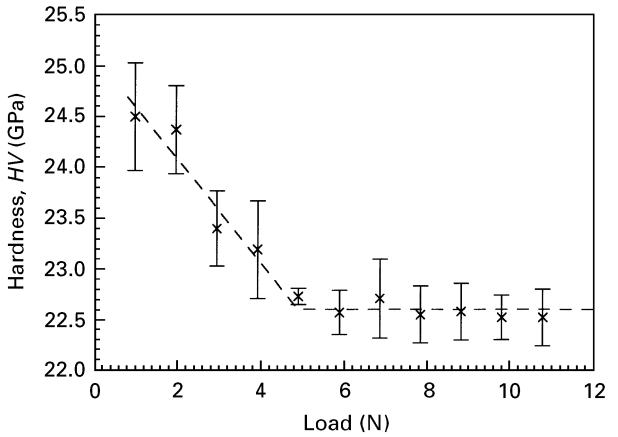

Figure 5 Hardness as a function of load for sintered α-SiC with a density of 3.11 $Mg\,m^{-3}$.

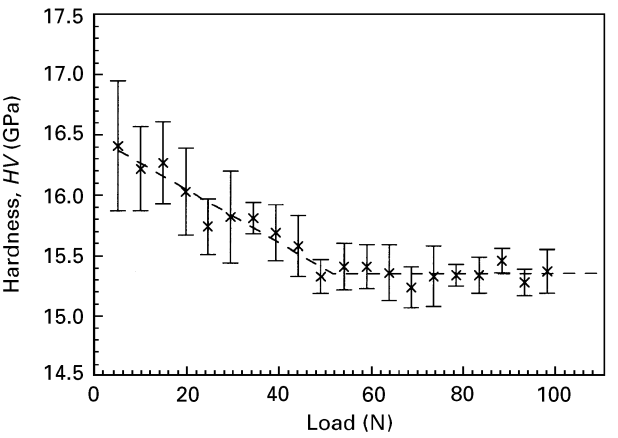

Figure 6 Hardness as a function of load for NC132 silicon nitride.

Equation 14 predicts $1/d_c$ should be proportional to B, and the experimental data, plotted in Fig. 9, confirm that there is a correlation for all materials over a broad range of diagonal size and material brittleness. The correlation supports the general form of the energy balance model for indentation. Of particular interest is the intersection of the linear regression line very near the origin, indicating a material with a brittleness value of zero would exhibit a fracture response at an infinite Vickers diagonal. The slope of the

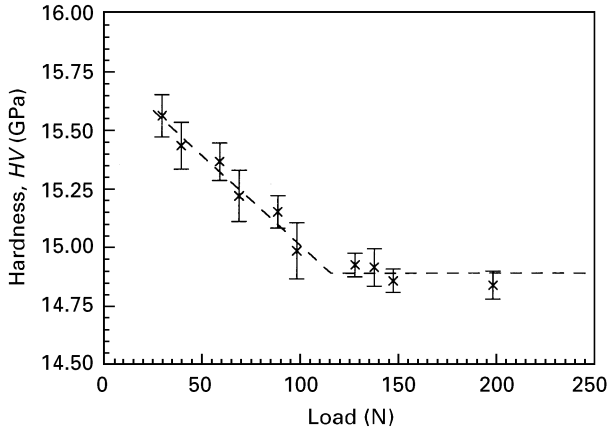

Figure 7 Hardness as a function of load for NBD200 silicon nitride.

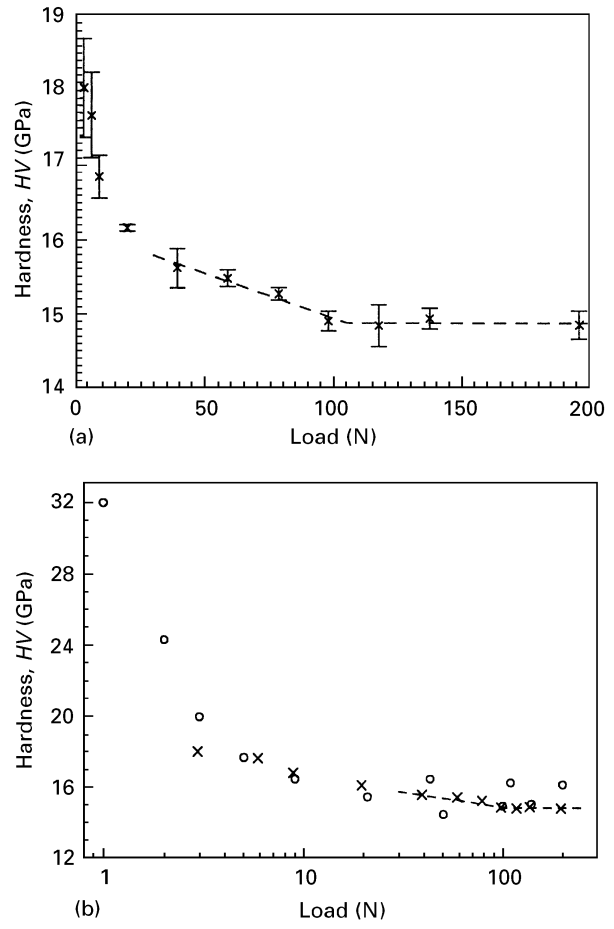

Figure 8 Hardness as a function of load for NT154 silicon nitride: (a) shows data on linear axes from the present study with uncertainty bars of one standard deviation, and (b) shows the same hardness (×) as well as data (○) from [9] superimposed. The dashed lines cover the same data range in both (a) and (b).

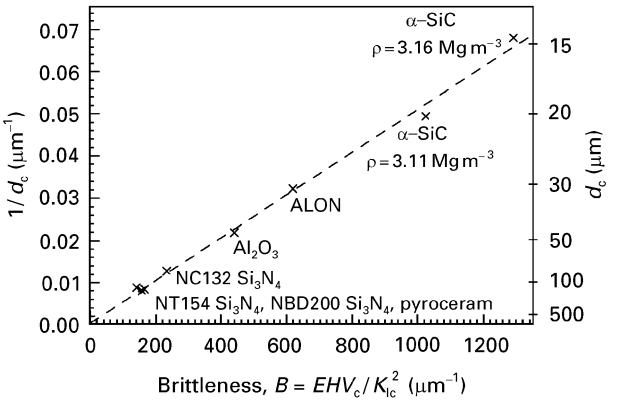

Figure 9 Graph of the reciprocal of the Vickers diagonal size at the transition point versus brittleness, B. The linear regression line passes through the origin, indicating that a material of zero brittleness will exhibit fracture behaviour at an infinite indentation size.

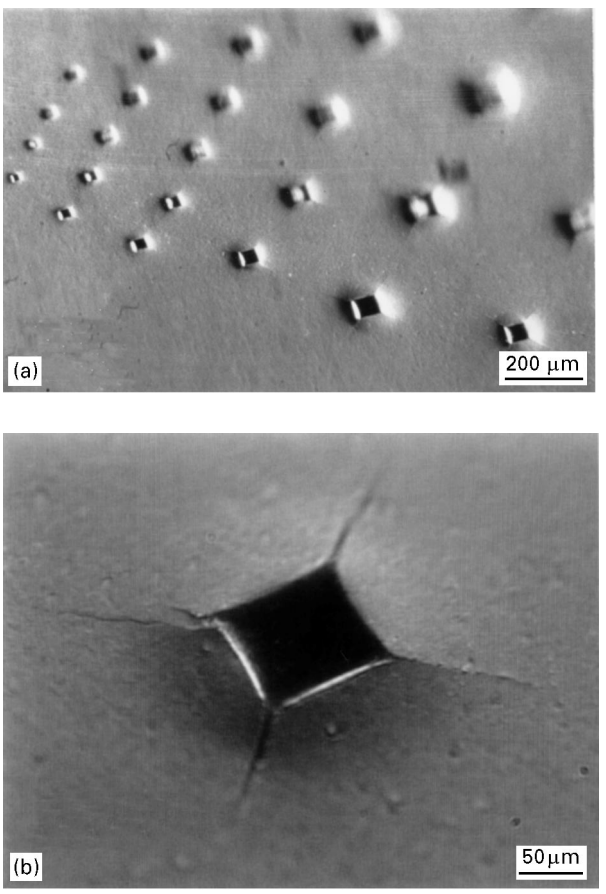

Figure 10 Indentations in NC 132 hot-pressed silicon nitride. Photos were taken with a stereo optical microscope with low-angle incident lighting and a severe specimen tilt so as to accentuate surface detail. The magnification markers are approximate only. (a) Shows rows of indents at different loads, from left to right: 9.8, 19.6, 29.4, 49, 98 and 73.5 N. (b) Shows a closeup of a 98 N indentation.

line, which is dimensionless, is 5.13×10^{-5}, and is a manifestation of the critical energy ratio, β_c, and the geometrical constants incorporated in A′ in Equation 14. The geometrical constants include the total fracture surface area, but this would be difficult to quantify independently.

Fig. 10 shows indentations in the hot-pressed silicon nitride at loads below and above the transition point. There are no obvious differences in the surface appearances of the indentations for this material at loads in the vicinity of P_c. Small cracks prior to the transition were noted in all the materials except the sintered silicon carbide, in which cracking was first observed at the transition point. Above P_c, however, surface cracking increased noticeably with load. This effect was more dramatic in materials with high brittleness ($B > 200\ \mu m^{-1}$), where different types of

cracks and surface damage rendered most indents unreadable beyond the highest loads shown in the corresponding figures. In these materials, reasonable diagonal measurements could be obtained for fewer than 25% of the indents made at the highest loads.

In most materials, the presence of fine cracks did not unduly obscure the indentation corners. At the highest loads, where cracking was more pronounced, the existence of displaced grains and lateral cracks required more judgement in rejecting indents and estimating the indentation sizes. Although the measured size variations were greater at the higher loads, this was not necessarily reflected in higher data scatter, because the greater overall dimensions of the indentations compensated for this scatter.

4. Discussion

Other investigators have realized that cracking is intimately involved with hardness measurements. Li *et al.* [12] noted that extensive cracking was associated with their hardness becoming load independent in sintered silicon carbide. They argued that the cracking is a process that substitutes for and limits the flow processes and thus interferes with attempts to measure a true hardness. Berriche and Holt [9] argued that the ISE was directly connected with cracking they measured at loads as low as 1 N in a series of silicon nitrides. Strong new corroborative evidence for the connection between the hardness transition and cracking was recently reported by Yurkov and Bradt [48] who used acoustic emission to monitor the indentation of five SiALON ceramics over a broad indentation load range. Their hardness–load curves did reach constant hardness plateaus, but at different magnitudes for the five materials. The fracture toughness ranged from 3.9 to 5.7 $MPa\,m^{-1/2}$ for the different compositions, and significant acoustic emission activity was first detected at the point where the plateaus were reached. Their graphs of P/d versus d also showed slight bends, presumably occurring at the transition points.

The sintered silicon carbide data warrant further explanation. There are two data points for this material in Fig. 9 and two separate data listings in Table I, corresponding to the data in our study and that reported by Li *et al.* [12]. The fracture toughness values were reported to be 3.0 $MPa\ m^{-1/2}$ in each study. Each team used the same test method (surface crack in flexure or controlled surface flaw). Ghosh *et al.* [58], in an extension of the Li *et al.* [12] study, also reported corroborative data from chevron notch tests and concluded the toughness for this material was 3.0 $MPa\,m^{-1/2}$ and that it exhibited flat R-curve behaviour. The materials in the two studies had different densities, however. The higher density material (3.16 $Mg\,m^{-3}$, 98% dense) used by Li *et al.* was harder and stiffer than the lower density material (3.11 $Mg\,m^{-3}$, 96% dense) we used in the present work. The brittleness parameter, B, is therefore higher for the higher density material, and the hardness transition point, d_c, is smaller as shown in Fig. 9. Seshadri *et al.* [64] also illustrated a load–hardness curve with a plateau for another batch of this material but there were insufficient data at the low loads to determine an exact transition point.

The hardness transition has similarities to other size transition correlations for fracture discussed in [32, 65–68]. In each case, the energy available from volume strain energy is balanced with the surface energy needed to propagate a crack. The strain energy scales with the volume of the body, whereas the energy required for crack extension increases with crack area. This gives rise to a cube/square size scaling that leads to a critical dimension or length. The critical length could be a specimen or crack size and determines whether a body behaves elastically (brittle), elastic–plastically or plastically (ductile). Puttick [65] stated: "… the critical length is proportional to the ratio of a surface free energy density to a volume free energy density". Critical sizes for these transitions can be devised for Hertzian contact problems [65], blunt or sharp indentation loadings [35, 66], notched or precracked tensile specimens [65, 67], or the peeling of metal–epoxy joints [67].

In our model of the hardness–load behaviour for ceramics, at low indentation loads energy is expended in volume strain energy deformation and surface energy processes. As the applied indentation load and the corresponding work of indentation are increased, the volume and surface terms rapidly increase with the cube/square dependencies until a transition occurs. New area in the form of escalated crack growth and/or the initiation of new types of cracking commences at the constant hardness transition point. Changes in the magnitude of frictional effects also result from cube/square scaling, but rapidly decrease in significance as the relative amount of new Vickers indentation surface area decreases with increasing indentation load. Extensive cracking following the constant hardness transition would also alleviate some of the frictional effects.

The surface energy consumed in cracking ($H_c - a'_2$ in Fig. 2) is relatively small in magnitude: i.e. the surface energy contribution to hardness due to the cracks, a'_1/d_c, must be very small compared to the volume energy contribution, a'_2. This is especially true if the transition to constant hardness and fracture orientated behaviour does not occur until large loads are applied, with resulting large Vickers impressions, as for less brittle materials. Eventually, however, even the most ductile material will exhibit a brittle fracture response when the load is high enough [67]. For more brittle materials, with a fracture response at smaller Vickers diagonals, a brittle transition should be somewhat more noticeable; i.e. $(H_c - a'_2)$ in Fig. 2 is larger. Fig. 5 for the sintered silicon carbide illustrates this. As small as the surface energy contribution may be, it is quite significant in determining the fracture parameters associated with brittle failure, and should be highlighted rather than ignored.

The materials evaluated in this study had hardness plateaus, but there may have been instances where insufficient energy was absorbed in the post-transition

region for such a plateau to occur. In such cases a change in the slope of hardness–load or hardness–diagonal sizes may occur once the massive cracking phase commences. One possible empirical model for this is included as Appendix I.

As an alternative to the linear hardness versus load graphs that we have presented, we reanalysed our results by the conventional methods to evaluate the ISE parameters to determine whether these methods could discern the transition point. Following the procedures of Fröhlich *et al.* [21], Frischat [27] and Li and coworkers [24, 25] P/d was plotted against d in accordance with Equation 4 with both sides divided by d. The line on such a plot will have a slope of a_2 and a y-intercept of a_1. Fig. 11 shows such a graph for the alumina, utilizing the same data as given in Fig. 3. A very good fit is obtained with a straight line with a correlation coefficient of 0.9996. A closer examination of Fig. 11 reveals that there is a subtle bend in the line at the constant hardness transition point of 46 μm (from Table I and Fig. 3). This very slight bend at the constant hardness transition point is barely perceivable in all similar graphs for the six materials in this study. Alternately, log–log graphs of P verus d (or vice versa) are used to determine the Meyer constant, n, in Equation 2. Lankford and Davidson [49] showed a graph of log-d versus log-P for the sintered α-SiC that completely masked the transition point in the middle of their data set. Clinton and Morrell [4] showed data for several aluminas that clearly illustrated a kink in their d versus P graph at the point where a transition to constant hardness occurred. Gahm [69] noted that a kink in P versus d curves was related to the first observed cracking in two glasses. Our point is that the conventional analyses of the ISE tend to overlook the existence of the transition point in the hardness curves.

Furthermore, the analysis to obtain the a_1 and a_2 constants for Equation 4 should only use the P–d data up to the transition point and not beyond. This is because the slopes of the P/d versus d plots for $d < d_c$, are all smaller than the slopes for $d > d_c$.

Figs 12 and 13 illustrate the shortcomings of the conventional ISE analysis very clearly. Equation 6 is graphed in these figures utilizing constants a_1' and a_2' determined from P/d versus d graphs for alumina and the hot-pressed silicon nitride, respectively. It is obvious that curves miss the abrupt transition to a constant hardness. This tendency for curve-fitting exercises to mask the actual hardness response of the material is exacerbated if the hardness data are plotted logarithmically, or are "normalized" or otherwise modified in a such a manner so as to inadvertently conceal a transition to constant hardness.

The hardness data curves in Figs 3–8 prior to the transition point are more linear than anticipated. They should exhibit some curvature due to the a_1/d or a_1'/d terms, but this curvature might be very slight for loads that are already past the bend in the ISE hyperbola, but below the transition point to constant hardness. In most of these figures, the data collected are at loads well above the low load, high ISE portion of the curves (which usually are below 10 N). The cold-rolled iron in [25] also exhibits a more linear response when frictional effects are alleviated. The hardness data in [10, 11, 17] follow a linear trend as well, in spite of the curves superimposed by the respective authors on their data. This suggests that the linear response is real

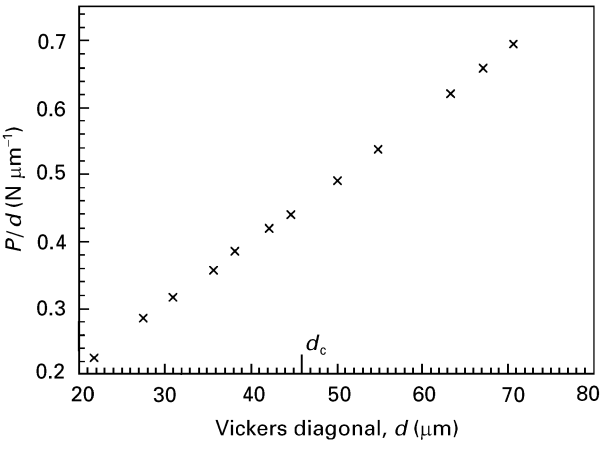

Figure 11 P/d versus d for AD999 alumina, using the same data in Fig. 3. The transition occurs at $d = 46$ μm.

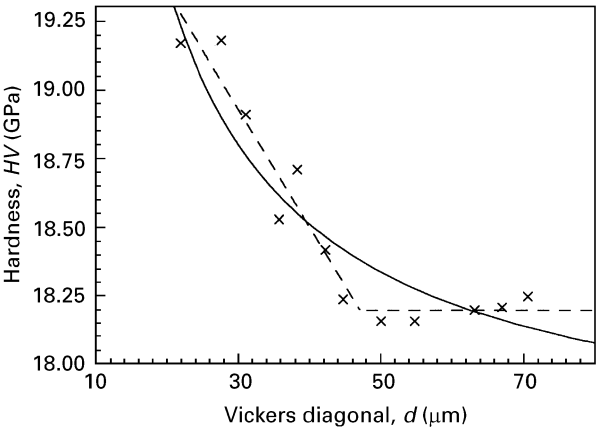

Figure 12 Hardness as a function of diagonal size for AD-999 alumina: (– – –) experimental data trend with a transition point, (——) best fit using Equation 6.

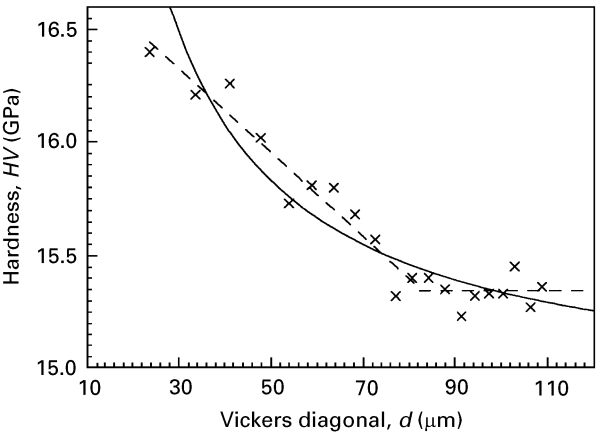

Figure 13 Hardness as a function of diagonal size for NC 132 silicon nitride: (– – –) experimental data trend with a transition point, (——) best fit using Equation 6.

and not unusual. Possible contributions to this effect are elastic recovery and material buildup around the edges of the indentations, such that a non-proportional relationship results between the Vickers diagonal and the penetration depth. Fig. 10 illustrates such a buildup. A possible contribution to the linearity of the hardness data is non-proportional crack growth prior to the brittle transition. These effects are not mutually exclusive and may be cumulative.

The generality of the transition point to constant hardness has yet to be confirmed for all brittle materials. The brittleness of most zirconias is so low ($B < 100\ \mu m^{-1}$) that transition points would not occur until indents were hundreds of micrometres in size, at very high indentation loads. This study has focused on dense polycrystalline ceramics. It is unclear whether a hardness transition point also occurs for porous materials because densification or crushing may be dominant. Berriche and Holt [9], however, reported data for porous silicon nitrides where such a transition was evident. Other complications may exist for glasses whereby structural densification is an important part of the indentation response, or for materials that undergo strain-induced phase transformations. For example, Ritter *et al.* [52] presented Vickers hardness versus load data for soda-lime glass that showed a transition point to constant hardness at approximately 5 N or a diagonal size of about 44 μm. This is somewhat larger than the expected 33 μm from Fig. 9 for this material, which has a B of $\sim 6 \times 10^8\ \mu m^{-1}$. Densification or phase transformations would contribute to the volume energy absorption terms in the energy balance, and could retard the onset of extensive cracking. Critical transition points and the β_c ratio may be different for these materials compared with the dense polycrystalline ceramics evaluated in this study. Alternate classes of materials may be represented by different slopes or curves on Fig. 9.

We conclude this section by noting that Knoop indentations exhibit much less cracking than Vickers indentations at the same load [12, 13, 48, 70]. Any possible constant hardness threshold due to a change in cracking scale may be suppressed until much higher loads, and in any case, may not even be noticeable. Knoop hardness–load curves gradually reach a constant hardness at very high loads and the Knoop plateau is usually lower than the Vickers plateau values (e.g. [12]). Thibault and Nyquist [71] noted that the onset of serious cracking led to a decrease in the apparent Knoop hardness. This may have been due in part to displacement of the indentation tips or sides, or as Swain and Wittling [26] have recently argued, the crack opening displacement under the Knoop indentation leading to greater indenter penetration.

4.1. Brittleness

Brittleness, B, has been defined here in terms of the material's hardness, Young's modulus, and fracture toughness, as

$$B \equiv \frac{H_c E}{K_{Ic}^2} = \frac{H_c}{G_{Ic}} = \frac{H_c}{2\gamma_f} \propto \frac{\text{deformation energy per unit volume}}{\text{fracture surface energy per unit area}} \quad (20)$$

where G_{Ic} is the critical strain energy release rate. As noted previously, H_c is not only hardness in units of force per unit area, but is directly proportional to the work per unit volume of deformation. The fracture surface energy, γ_f, is the energy necessary to create unit fracture surface area. Thus the brittleness, B, compares deformation to fracture processes. A material with a low B is more apt to deform than fracture, and conversely, a material with a high B is more apt to fracture. B increases with both hardness and stiffness, and decreases rapidly with increasing fracture toughness. Pyroceram, for example, has a relatively low hardness and Young's modulus compared with other ceramics, but its low fracture toughness renders it a B value similar to that for silicon nitride. The roles of the respective components in B are not difficult to appreciate. A material with a high H, when indented with a penetrator, is more resistant to deformation that would otherwise distribute the load and alleviate the stress concentration. The concentrated stresses are more apt to cause cracking. Similarly, a high Young's modulus means the material is also rigid and unable to distribute the indentation forces, which should also promote cracking. Conversely, a high fracture toughness or fracture surface energy in the denominator indicates a greater resistance to cracking. Materials with a low K_{Ic} or γ_f will crack more readily.

The generic H_c term in Equation 20 ideally should include only deformation energy such as the a_2' term, but this requires data reduction and analysis. (The plateau Knoop hardness, HK_c, might be more suitable because cracking is much reduced with Knoop indentations, but much higher loads are needed to reach the Knoop plateau.) It is more practical and convenient to use HV_c, the plateau Vickers hardness in tabulations of B as we have done in this paper using Equation 15, although HV_c incorporates some fracture energy as well as deformation energy. The fraction of the total energy that is in the latter form is, however, small, despite the importance of the fracture component to the indentation response.

The Mode I fracture toughness (opening or tensile mode) is used in our definition of B although we acknowledge that Mode II (sliding) and Mode III (tearing) loading may contribute to fracture. Mode II loadings are certainly involved in the field underneath an indentation. The extent of K_{IIc} and K_{IIIc} contributions will depend to a great deal upon the local stress states and, in any case, it is not unreasonable to assume that K_{IIc} and K_{IIIc} may scale in magnitude with K_{Ic}.

From Equation 14, it can be seen that the brittleness, B, is inversely proportional to the size of an indentation needed to induce brittle behaviour that we previously showed was related to the cube/square

scaling phenomenon. This is analogous to a brittleness measurement proposed by Mouginot [66] in which brittleness is inversely proportional to the size of a ball or punch needed to induce brittle behaviour. The definitions are therefore quite similar. Lawn and Marshall [32] similarly noted the size scaling and related it to whether indentations at a given load were characterized primarily by plastic deformation or by whether fracture had commenced.

4.1.1. Other brittleness parameters

Brittleness in a general sense may have any one of a number of meanings, and a variety of techniques or parameters that have been proposed to characterize brittleness are listed in Table II. Early attempts to define brittleness were primarily concerned with single crystals. Parameters were chosen for theoretical relevance rather than possible practical applications.

A variety of engineering definitions arose in connection with hardness testing. For example, in his book on hardness, Mott [31] stated that the occurrence and extent of cracking around indentations was a quantitative inverse measure of brittleness. Lysaght [72] stated that brittleness could be appraised by measuring the first load to cause fracture in Knoop indentations. Softer glasses were much less brittle than harder glasses. Bernhardt [22] defined brittleness as the inverse of the Vickers indent diagonal size that just caused one crack to form on the average and showed data for seven glasses. Thibault and Nyquist [71] suggested that cracking around a Knoop indentation could be classified by six classes at a given load and that this could categorize brittleness. In a discussion of that paper, Winchell [73] indicated that brittleness or friability could be defined as the minimum load to cause fracture or cracking consistently. Shuvalov [74] proposed a very similar scheme to Thibault and Nyquist's.

The advent of fracture mechanics has led to new materials parameters to characterize brittleness of elastic bodies including fracture surface energy, γ_f, from the Griffith model, and critical stress intensity factor, K_{Ic}, or the critical strain energy release rate, G_{Ic}. The first two of these are routinely characterized today. K_{Ic} or γ_f alone are not always sufficient to characterize the brittleness of a material completely, however. The sintered silicon carbide in Table I illustrates this very well. Both silicon carbides were obtained from the same source, but although they had different densities, they possessed identical fracture toughnesses. This is not surprising because this silicon carbide fractures transgranularly. The small amount of porosity (2 or 4% by volume for the two batches) did not affect the fracture toughness. The brittleness of

TABLE II Brittleness indices [the brittleness increases with an increase in the listed parameter, unless marked with an asterisk (*), which denotes an inverse relationship]

Reference	Parameter	Comment
Irwin [75]	K_{Ic}^*	Critical stress intensity factor, Mode I
Griffith [76]	γ_f^*	Fracture surface energy $\gamma_f = K_{Ic}^2(1-\nu^2)/2E$ (plane strain)
Irwin [75]	G_{Ic}^*	Critical strain energy release rate, $G_{Ic} = 2\gamma_f$
Kelly *et al.* [77]	σ/τ^*	Compares theoretical cleavage strength, σ, to theoretical shear strength, τ, in single crystals
Rice and Thomson [78]	$\mu b/\gamma_f$	Shear modulus, μ, times Burger's vector, b, divided by fracture surface energy, γ_f. Determines whether a crack in a single crystal is atomically sharp or blunt due to dislocation generation when stress is applied
Gogosti [79, 80]	$X = (\sigma_u^2/2E)\int\sigma d\varepsilon$	The area under the stress–strain curve up to failure if the material were completely elastic, normalized by the actual area under the stress–strain curve to failure, X is equal to 1 for linearly elastic brittle ceramics
Lawn *et al.* [40]	$H^2/G_{Ic}E$ or H^2/K_{Ic}^2	G_{Ic} is the strain energy release rate. When expressed in terms of E and K_{Ic}, this index of brittleness is similar to the next index
Puttick [65]	$E\gamma_f/\sigma_y^{2*}$ or K_{Ic}^2/σ_y^{2*}	σ_y is the yield stress, i.e. the ratio of the surface energy associated with fracture to the volume strain energy If σ_y is proportional to H (e.g. for a perfectly plastic material, $H = 3\sigma_y$), then Puttick's index is the inverse of the Lawn [42] index listed above[a]
Lawn and Marshall [32, 39]	H/K_{Ic}	Vickers hardness divided by stress intensity. This is the square root of the index listed above; developed for convenient comparison rather than a theoretical basis
Mouginot [66]	$a_t \propto E\gamma_f/H^{2*}$ [or $\propto E^2\gamma_f/H^3$]*	Brittleness is determined by the size, a_t, of a flat (or spherical) punch needed to induce brittle behaviour (Hertzian cone cracks) rather than plastic deformation
Quinn and Quinn This paper	$B = EH_c/K_{Ic}^2$	Ratio of indentation work (or work of deformation) to fracture energy; this can be related to the onset of extensive fracture via a critical length
Sehgal *et al.* [81]	c/d	Ratio of crack length, c, to indent size, d, for Vickers indents at a specified load; empirically related to H/K_{Ic}

[a] In a footnote, Puttick credits Irwin (1958) for having first recognized the significance of the parameter $E\gamma_f/\sigma_y^2$ particularly as it is a measure of crack tip plasticity and governs the transition from plane stress to plane strain fracture, which is yet another size transition.

the two batches varied because E and H differed. These latter parameters are much more sensitive to the density difference.

Various combinations of hardness, stiffness, fracture toughness and other parameters have been used to indicate a degree of brittleness. Some of the definitions are listed in Table II. The parameters developed by Puttick [65], Mouginot [66] and Lawn and associates [40] are very similar, and indeed, have the same relationship of hardness, Young's modulus and fracture energy or fracture toughness. This should not be surprising because all trace their roots to an energy balance whereby crack formation or propagation entails conversion of strain energy to fracture surface energy, analogous to the Griffith model. The specific loading configurations and geometries modelled vary somewhat, but inevitably internal strain energy, $\sigma^2/2E$, is converted to fracture energy. The stress squared term usually is converted to a yield stress squared term, which is then converted to hardness squared. The fracture energy and Young's modulus are converted to a K_{Ic} term

$$(\sigma^2/2E) \times \text{volume} \rightarrow 2\gamma_f \times \text{area}$$

or

$$(\sigma^2/2E) \rightarrow 2\gamma_f/D$$

and

$$D \propto (\gamma_f E)/\sigma^2$$

where D is a characteristic dimension such as the crack size. If plastic deformation occurs, then $\sigma = \sigma_y \propto H$, and then

$$D \propto (\gamma_f E)/H^2 \propto K_{Ic}^2/H^2$$

The importance of the H/K_{Ic} or σ_y/K_{Ic} ratio in indentation fracture was recognized by Evans and Wilshaw [35], who stated that the higher the H, the larger the cracks from corners of Vickers indentations. The H/E ratio also appeared in their paper and was related to the force necessary for a spherical indentor of a given size to cause plastic flow. Lawn, Marshall, Evans and coworkers expanded the fracture mechanics modelling in a series of papers and eventually in [32, 39, 40] they compared the different load dependencies of crack size and indentation impression size that led them to propose H^2/K_{Ic}^2 or H/K_{Ic} as an "index of brittleness". These ratios, which were utilized as a convenient basis for materials classification [32], repeatedly occur in various equations for the initiation or propagation of the specific, idealized crack models. These were used to prepare fracture-deformation maps that delineate "deformation controlled" versus "fracture controlled" behaviour [34].

Our alternative brittleness parameter, $(H_c E)/K_{Ic}^2$ was derived from an energy ratio or balance at the hardness plateau. It is very similar to the H^2/K_{Ic}^2 or σ_y^2/K_{Ic}^2 ratios cited above, but incorporates E rather than another H. H and E have the same dimensions (force/length^2) and the respective brittleness parameters also have the same dimensions, which are length^{-1}. Unlike the H^2/K_{Ic}^2 or σ_y^2/K_{Ic}^2 ratios, B is not coupled to any specific, idealized crack model. The critical plateau loads, P_c, are well above the threshold loads, P^*, for initiation of the idealized median, radial or lateral cracks according to conventional indentation fracture models [34, 43, 44]. There is, however, a connection between B and indentation crack models, thus a short review of indentation fracture mechanics is helpful.

Evans and Wilshaw [35] suggested that comparisons of measured crack lengths, c, and indentation sizes, d, (i.e. c/d ratios) could be developed into a method of measuring fracture toughness. Evans and Charles [36] pursued this, and using a dimensional analysis, realized that the c/d ratio related well to $K_{Ic}/(Hd^{-1/2})$, but only if a correction factor of $(H/E)^{0.4}$ was applied, so that $(c/d) \propto (K_{Ic}/Hd^{1/2})\,(H/E)^{0.4}$. The material constants in the latter expression are $K_{Ic}/(H^{0.6}E^{0.4})$, which is very close to our B. Lawn *et al.* [44] modified the earlier models by showing that the ratio of the radius of the plastic zone to the radius of the indentation contact area was not constant but varied with $(E/H)^{1/2}$. The relationship for crack size, c, and indent size, d, then became [44]

$$\left(\frac{K_{Ic}}{Hd^{1/2}}\right)\left(\frac{H}{E}\right)^{1/2} \propto \left(\frac{c}{d}\right)^{-3/2} \tag{21}$$

This representation with K_{Ic} normalized by H, and H normalized by E, has become the norm in the ceramics indentation fracture literature. The $(H/E)^{1/2}$ term is usually incorporated along with geometrical terms into a χ_r term that describes the residual stress driving force for crack extension [34].

We observe that Equation 21 can easily be rewritten

$$\left(\frac{HE}{K_{Ic}^2}\right) \propto \frac{c^3}{d^4} \tag{22}$$

So, nestled amidst dozens of relationships for crack size, indentation size, hardness, load, fracture toughness and assorted geometrical constants, it becomes apparent that B has been an important factor in indentation fracture mechanics all along. It seems reasonable that a parameter for brittleness of a material should incorporate Young's modulus of the material.

4.1.2. Future work

Further work could be aimed at correlating B with other fracture-deformation processes that may be characterized by critical lengths or dimensions. Brittleness, B, may be useful in characterizing erosion, scratch, impact and wear resistances as well as the machinability of brittle materials. In each case, the ratio of deformation energy to fracture energy may be important and could herald shifts in behaviour as critical thresholds in controlling parameters are exceeded. B may not necessarily be useful in instances where the loading is purely elastic: e.g. a plate with a crack loaded to fracture in tension or thermal shock fracture, in which case K_{Ic} or γ_f may be eminently suitable.

B^{-1} has units of length and for the materials in our study ranges from 0.8 to 7.0×10^{-9} m. Different

proportionality constants (e.g. Equation 13) will be applicable depending upon the specific loading condition and these could be difficult to derive other than by empirical means.

In principle, fracture toughness may be evaluated by measuring the hardness–load curves to find the hardness transition point. The plateau hardness, H_c, and Young's modulus, E, along with d_c can be used in conjunction with Equation 14 or Fig. 9 to solve for K_{Ic}. We are hesitant to propose yet another indentation method for this purpose, but this procedure could be very useful for characterizing small specimens or single crystals. Much further work needs to be done, however, to verify the universality of this approach and to establish the uncertainty estimates of using this method. Accurate and precise hardness readings will be essential.

The accuracy and precision of the hardness transition point measurement depends upon the brittleness of the material. This is illustrated in Fig. 14. Harder and more brittle materials have a transition at lower load values and it is easy to detect the sudden change in slope of the hardness–load curve. Fig. 5 (silicon carbide) and the aluminum oxynitride data in [16] are good examples. On the other hand, less brittle materials have transitions at higher loads, and much greater care is needed to measure the data accurately just before and after the transition. Figs 3 (alumina), 4 (Pyroceram) and 6–8 (silicon nitrides) demonstrate this clearly. For the less brittle materials, diagonal length readings accurate to within 1.0 μm, and preferably 0.5 μm are essential. Experimental scatter must be carefully controlled lest the transition be obscured. A minimum of five measurable indentations are recommended at each load, and as we have noted before, this may require quite a few indentations at the higher loads. For all materials, brittle or not, hardness should be measured over a broad load range, and results should be plotted on linear (not logarithmic) axes. Offset hardness axes such as shown in Figs 3–8 are recommended. Uncertainty bars are essential.

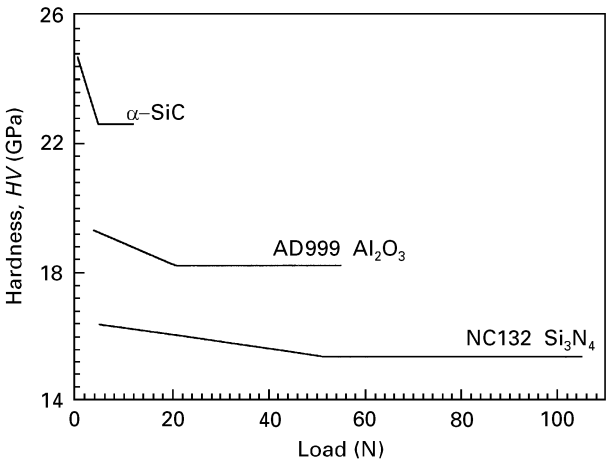

Figure 14 Hardness–load curves for silicon carbide and silicon nitride. The carbide, which is harder and more brittle, has a transition at a lower load. The transition is sharper and easily detected. The nitride transition is at a higher load and requires more careful measurements to characterize.

Fig. 8 illustrates some of these recommendations. The transition is readily evident in Fig. 8a, which emphasizes the data at the intermediate and higher loads. On the other hand, Fig. 8b shows the same data with a logarithmic horizontal axis and with additional results from Berriche and Holt [9]. The higher scatter in the latter data and the logarithmic axis overemphasizes the low load, high hardness data and the transition point at 105 N is obscured or lost.

It often is necessary to use different hardness machines for different load ranges. This should be done with caution because bias between machines may exist. Universal strength testing machines should be avoided or used with extreme caution because hardness is very sensitive to loading rate and vibration. It may be suitable to use more than one hardness machine to create the indentations, but then utilize only one instrument for the diagonal size measurements. We estimate that, with appropriate care, transition points in terms of indentation load can be measured to within $\pm$ 10%.

5. Conclusions

Vickers hardness–load curves for a number of brittle ceramics exhibit a distinct transition to a plateau constant hardness level that corresponds well to a relationship between hardness, Young's modulus and fracture toughness. A new index of brittleness, $B \equiv (HE)/K_{Ic}^2$, has been proposed that is derived from deformation and fracture energy ratios and correlates well with the observed hardness transition points. Besides providing a practical scale for material comparisons, the brittleness parameter, B, has potential predictive value in research and ceramic design applications.

Appendix

One possible energy balance for $d > d_c$, based on Equation 7, is

$$Pd = a_1 d^2 + a_2 d^3 + a_3 (d - d_c)^2 \qquad \text{(A1)}$$

where the additional $a_3(d - d_c)^2$ term represents fracture surface energy consumed by a new system of cracking at $d > d_c$. The fracture surface area for the new crack system is assumed to scale with $(d - d_c)$. Re-expressing Equation A1 in units of hardness

$$\frac{P}{d^2} = \frac{a_1}{d} + a_2 + a_3 \frac{(d - d_c)^2}{d^3} \qquad \text{(A2)}$$

or

$$H = \frac{a_1'}{d} + a_2' + a_3' \frac{(d - d_c)^2}{d^3} \qquad \text{(A3)}$$

Fig. A1 illustrates both the pre- and post-transition point behaviour as functions of indentation diagonal size. The last term of Equation A3 (which is also plotted separately on the bottom of this figure) gradually rises from a value of zero at $d = d_c$ to a maximum of $0.15a_3$ at $d = 3d_c$ and then gradually

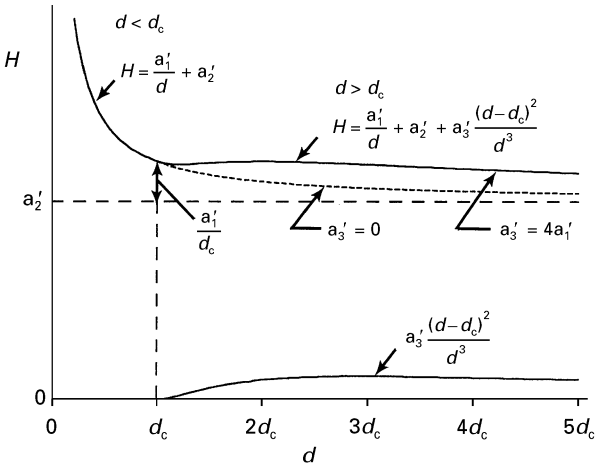

Figure A1 Hardness as a function of diagonal size according to Equation 23. The magnitude of a_3' determines whether the hardness is constant ($a_3' \sim 4a_1'$) or decreases ($a_3' \sim 4a_1'$) past the transition point.

diminishes. The effect of this term upon H depends upon the relative magnitudes of a_1' and a_3'. If $a_3' \sim 4a_1'$, the hardness is nearly constant over a broad range of indentation sizes as shown in the Figure. a_3' values less than this will lead to hardness diminishing with increasing diagonal size. The case of $a_3' = 0$ is also illustrated. Both the a_1' and a_3' terms incorporate the material's fracture surface energy, but the magnitude of the latter term is expected to be higher because there would be much greater actual surface area created by the massive cracking associated with the post-transition fracture term. Experimental hardness data with a gradual decrease in H past the transition point have been shown for alumina by Clinton and Morrell [3]. This could be related to a rising R-curve behaviour, in which case less cracking occurs than for more brittle materials with a flat R-curve.

Acknowledgements

The authors wish to thank Mr R. Gettings and Ms S. Tucker of NIST for assistance with hardness testing. G. Quinn thanks Dr W. Braue and the German Aerospace Research Institute in Cologne, Germany, for the opportunity to study fracture toughness and hardness relationships during a brief sabbatical visit in 1993.

References

1. P. M. SARGENT and T. F. PAGE, *Proc. Brit. Ceram. Soc.* **26** (1987) 209.
2. H. LI and R. C. BRADT, *J. Non-Cryst. Solids* **146** (1992) 197.
3. D. J. CLINTON and R. MORRELL, *Mater. Chem. Phys.* **17** (1987) 461.
4. *Idem.* in "Ceramic surfaces and surface treatments", edited by R. Morrell and M. Nicholas, British Ceramics Proceedings, No. 34, August 1984 (British Ceramics Society, Shelton, 1984) pp. 113–27.
5. I. J. McCOLM, "Ceramic hardness" (Plenum, New York, 1990).
6. P. M. SARGENT, in "Microindentation techniques in materials, science and engineering", edited by P. Blau and B. Lawn, ASTM STP 889, (American Society for Testing Materials, Philadelphia, PA, 1986) pp. 160–74.
7. V. E. LYSAGHT, "Indentation hardness testing" (Reinhold, New York, 1949).
8. H. BÜCKLE, *Metall. Rev.* **4** (1959) 49.
9. R. BERRICHE and R. T. HOLT, *J. Amer. Ceram. Soc.* **76** (1993) 1602.
10. G. N. BABINI, A. BELLOSI and C. GALASSI, *J. Mater. Sci.* **22** (1987) 1687.
11. J. J. PETROVIC, *J. Amer. Ceram. Soc.* **66** (1983) 277.
12. Z. LI, A. GHOSH, A. KOBAYASHI and R. C. BRADT, *ibid.* **72** (1989) 904.
13. J. E. RITTER, JR, F. M. MAHONEY and K. JAKUS, in "Fracture mechanics of ceramics", Vol. 8, edited by R. C. Bradt, A. G. Evans, D. P. H. Hasselman and F. F. Lange (Plenum, New York 1986) pp. 213–23.
14. D. J. GODFREY and K. C. PITMAN, in "Ceramics for high performance applications", edited by J. J. Burke, A. E. Gorum and R. N. Katz (Brook Hill, Chestnut Hill, MA, 1974) pp. 425–44.
15. J. T. CZERNUSZKA and T. F. PAGE, in "Ceramic surfaces and surface treatments", edited by R. Morrell and M. Nicholas, British Ceramics Proceedings, No. 34, August 1984 (British Ceramics Society, Shelton, 1984) pp. 145–56.
16. G. D. QUINN, N. D. CORBIN and J. W. McCAULEY, *Bull. Amer. Ceram. Soc.* **63** (1984) 723.
17. K. BALAKRISHNAN, J. KUMAR, P. RAMASAMY and G. ATTOLINI, *J. Mater. Sci. Lett.* **14** (1995) 720.
18. C. HAYS and E. G. KENDALL, *Metallography* **6** (1973) 275.
19. H. BÜCKLE, "Mikrohärteprüfung" (Berliner Union Verlag, Stuttgart, 1965).
20. R. MITSCHE, *Osterr. Chem. Z.* **49** (1948) 186.
21. F. FRÖHLICH, P. GRAU and W. GRELLMANN, *Phys. Status Solidi* (*a*) **42** (1977) 79.
22. E. O. BERNHARDT, *Z. Metallkde* **33** (1941) 135.
23. K. HIRAO and M. TOMOZAWA, *J. Amer. Ceram. Soc.* **70** (1987) 497.
24. H. LI and R. C. BRADT, *J. Mater. Sci.* **28** (1993) 917.
25. H. LI, A. GHOSH, Y. H. HAN and R. C. BRADT, *J. Mater. Res.* **8** (1993) 1028.
26. M. SWAIN and M. WITTLING, in "Fracture mechanics of ceramics", Vol. 11, edited by R. C. Bradt, D. P. H. Hasselman, D. Munz, M. Sakai and V. Ya Shevchenko (Plenum, New York, 1996).
27. G. H. FRISCHAT, in "Strength of inorganic glass", edited by C. Kurkjian (Plenum, New York, 1986) pp. 135–45.
28. D. R. TATE, *Trans. ASM* **35** (1945) 374.
29. R. ROESKY and J. R. VARNER, *J. Amer. Ceram. Soc.* **74** (1991) 1129.
30. A. PAJARES, F. GUIBERTEAU, A. DOMINGUEZ-RODRIGUEZ and A. H. HEUER, *ibid.* **71** (1988) C332.
31. B. W. MOTT, "Micro-indentation hardness testing" (Butterworth, London, 1956).
32. B. R. LAWN and D. B. MARSHALL, *J. Amer. Ceram. Soc.* **62** (1979) 347.
33. K. NIIHARA, R. MORENA and D. P. H. HASSELMAN in "Fracture mechanics of ceramics", Vol. 5, edited by R. C. Bradt, A. G. Evans, D. P. H. Hasselman and F. F. Lange (Plenum, New York, 1983) pp. 97–105.
34. G. R. ANSTIS, P. CHANTIKUL, B. R. LAWN and D. B. MARSHALL, *J. Amer. Ceram. Soc.* **64** (1981) 533.
35. A. G. EVANS and T. R. WILSHAW, *Acta Metall.* **24** (1976) 939.
36. A. G. EVANS and E. A. CHARLES, *J. Amer. Ceram. Soc.* **59** (1976) 371.
37. D. B. MARSHALL, *ibid.* **66** (1983) 127.
38. J. J. PETROVIC, L. A. JACOBSON, P. K. TALTY and A. K. VASUDEVAN, *ibid.* **58** (1975) 113.
39. D. B. MARSHALL and B. R. LAWN, in "Microindentation techniques for materials science and engineering", ASTM STP 889, edited by P. Blau and B. Lawn (American Society for Testing Materials, Philadelphia, PA, 1986) pp. 26–40.
40. B. R. LAWN, T. JENSEN and A. ARORA, *J. Mater. Sci. Lett.* **11** (1976) 573.
41. B. R. LAWN and A. G. EVANS, *J. Mater. Sci.* **12** (1977) 2195.
42. B. R. LAWN in "Strength of inorganic glass", edited by C. R. Kurkjian (Plenum, New York, 1986) pp. 67–86.

43. D. B. MARSHALL, B. R. LAWN and A. G. EVANS, *J. Amer. Ceram. Soc.* **65** (1982) 561.
44. B. R. LAWN, A. G. EVANS and D. B. MARSHALL, *ibid.* **63** (1980) 574.
45. W. C. OLIVER and G. M. PHARR, *J. Mater. Res.* **7** (1992) 1564.
46. R. BERRICHE and R. T. HOLT, *Ceram. Engng Sci. Proc.* **14** (1993) 188.
47. E. SÖDERLUND, I. REINECK and D. J. ROWCLIFFE, *J. Mater. Res.* **9** (1994) 1683.
48. A. L. YURKOV and R. C. BRADT, in "Fracture mechanics of ceramics", edited by D. Munz (Plenum, New York, 1996).
49. J. LANKFORD and D. L. DAVIDSON, *J. Mater. Sci.* **14** (1979) 1662.
50. R. F. COOK and G. M. PHARR, *J. Amer. Ceram. Soc.* **73** (1990) 787.
51. J. T. HAGAN and M. V. SWAIN, *J. Phys. D.: Appl. Phys.* **11** (1978) 2091.
52. J. E. RITTER, Jr, F. M. MAHONEY and K. JAKUS, in "Fracture mechanics of ceramics", Vol. 8, edited by R. C. Bradt, A. G. Evans, D. P. H. Hasselman and F. F. Lange (Plenum, New York, 1986) pp. 213–23.
53. D. LEWIS, III, *Bull. Amer. Ceram. Soc.* **61** (1982) 1208.
54. R. L. HALLSE, J. R. KOENIG and H. S. STARRETT, *Ceram. Engng Sci. Proc.* **2** (1981) 553.
55. R. J. GETTINGS and G. D. QUINN, *Ceram. Engng Sci. Proc.* **16** (1995) 539.
56. G. D. QUINN, R. J. GETTINGS and J. J. KÜBLER, in "Fracture mechanics of ceramics", edited by D. Munz (Plenum, New York, 1996).
57. G. D. QUINN, "Characterization of turbine ceramics after long-term environmental exposure", US Army Materials and Mechanics Research Center, Technical Report TR 80–15, April 1980.
58. A. GHOSH, M. G. JENKINS, K. W. WHITE, A. S. KOBAYASHI and R. C. BRADT, *J. Amer. Ceram. Soc.* **72** (1989) 904.
59. J. H. WESTBROOK and P. J. JORGENSEN, *Trans. AIME* **233** (1965) 425.
60. D. M. BUTTERFIELD, D. J. CLINTON and R. MORRELL, "The VAMAS hardness tests round-robin on ceramic materials", VAMAS Report No. 3 (National Physical Laboratory, Teddington, 1989).
61. R. J. GETTINGS, G. D. QUINN, A. W. RUFF and L. K. IVES, *Ceram. Engng Sci. Proc.* **15** (1994) 817.
62. *Idem*, *VDI Bericht* **1194** (1995) 255–64.
63. D. J. CLINTON, L. A. LAY and R. MORRELL, in "Special Ceramics", Vol. 8, edited by S. Howlett and D. Taylor (British Ceramics Proceedings, No. 37, Institute of Ceramics, Shelton, 1986).
64. S. G. SESHADRI, M. SRINIVASAN and L. KING, *Ceram. Engng Sci. Proc.* **4** (1983) 853.
65. K. E. PUTTICK, *J. Phys. C.* **13** (1980) 2249.
66. R. MOUGINOT, *J. Amer. Ceram. Soc.* **71** (1988) 658.
67. A. G. ATKINS and Y. M. MAI, *J. Mater. Sci.* **21** (1986) 1093.
68. B. R. LAWN and E. R. FULLER, *ibid.* **10** (1975) 2016.
69. J. GAHM, *VDI Bericht* **160** (1972) 25.
70. F. KNOOP, C. G. PETERS and W. B. EMERSON, *J. Res. NBS* **23** (1939) 39.
71. N. W. THIBAULT and H. L. NYQUIST, *Trans. ASM* **38** (1947) 271.
72. V. E. LYSAGHT, *Bull. ASTM* No. 138 **January** (1946) 39.
73. H. WINCHELL, *ibid.* **January** (1946) 327.
74. L. A. SHUVALOV, "Modern crystallography, Vol. IV, Physical properties of crystals (Springer-Verlag, Berlin, 1981) pp. 173–5.
75. G. R. IRWIN, "The encyclopedia of physics", Vol. VI (Springer, Heidelberg, 1958).
76. A. A. GRIFFITH, *Phil. Trans. Roy. Soc. A* **221** (1920) 163.
77. A. KELLY, W. R. TYSON and A. H. COTTRELL, *Phil. Mag.* **15** (1967) 567.
78. J. R. RICE and R. THOMSON, *ibid.* **29** (1974) 73.
79. G. A. GOGOTSI, *Ceram. Int.* **15** (1989) 127.
80. *Idem*, *J. Eur. Ceram. Soc.* **7** (1991) 87.
81. J. SEHGAL, Y. NAKAO, H. TAKAHASHI and S. ITO, *J. Mater. Sci. Lett.* **14** (1995) 167.

Received 25 March 1996
and accepted 10 February 1997